Available online at www.sciencedirect.com
ScienceDirect
International Journal of Heat and Mass Transfer 50 (2007) 2236–2245
International Journal of HEAT and MASS TRANSFER
www.elsevier.com/locate/ijhmt

# Melting and resolidification of a subcooled metal powder particle subjected to nanosecond laser heating

Chad Konrad [1], Yuwen Zhang *, Yu Shi

*Department of Mechanical and Aerospace Engineering, University of Missouri – Columbia, Columbia, MO 65211, USA*

Received 25 January 2006; received in revised form 28 October 2006
Available online 28 December 2006

**Abstract**

Melting and resolidification of a subcooled spherical metal powder particle subjected to nanosecond laser heating are investigated analytically. The problem is divided into three stages: preheating, melting and resolidification, and thermalization. The temperature distributions in the liquid and solid regions and the location of the solid–liquid interface are obtained using an integral approximate method. The effects of the laser intensity and pulse width, initial subcooling, and particle radius on the melting and resolidification of powder particles were investigated. The Selective Laser Sintering (SLS) process for a pulsed laser can be simulated by repeating the three stages but varying the initial conditions.


## 1. Introduction

Selective Laser Sintering (SLS) is an emerging technology that can build structurally-sound parts from powdered material via layer-by-layer sintering (for amorphous powder, such as polycarbonate) or melting (for crystalline powder, such as metal) induced by a directed laser beam. Amorphous powder particles are sintered by the glass transition phenomenon, which occurs at a relatively low temperature, while metallic powder particles are joined via melting and resolidification, which of course requires the particle surface temperature to briefly exceed its melting point. SLS is a very useful rapid manufacturing method because it allows for the manufacture of complex parts often unobtainable by more common manufacturing processes [1,2]. During a metal powder SLS process the surface of the powder bed is scanned with a laser beam to melt the powder and as the beam moves away the liquid resolidifies into a solid. Another layer of powder is then pushed over the newly solidified surface and the process is repeated, thus building a solid object layer by layer. A review of the most recent SLS advances as reported in various journals and proceedings is presented by Kumar [3].

There are other obstacles that must also be overcome before SLS can be used for mass production of final, high quality parts that exhibit good surface finish and desirable mechanical properties. One such obstacle is the balling phenomenon [4], in which melted powder grains stick to each other via surface tension forces, thereby forming a series of spheres with diameters approximately equal to the diameter of the laser beam. One way that the balling phenomenon can be combated is to use a powder bed consisting of two different types of metal powder, one with a significantly higher melting point than the other as suggested by Bunnell [5] and Manzur et al. [6]. Melting and resolidification of the low-melting point powder are the mechanism by which high-melting point powder particles are bonded together.

The fundamentals of melting and solidification have been investigated extensively and are well documented [7–9]. Yilbas [10] has presented a numerical solution for a pulsed $CO_2$ laser heating process. Rostaml and Raisi [11] have numerically solved the temperature distribution and

* Corresponding author. Tel.: +1 573 884 6936; fax: +1 573 884 5090.
*E-mail address:* zhangyu@missouri.edu (Y. Zhang).
[1] Present address: Buro Happold, 100 Broadway, 23rd Floor, New York, NY 10005, USA.

0017-9310/$ - see front matter © 2006 Elsevier Ltd. All rights reserved.
doi:10.1016/j.ijheatmasstransfer.2006.10.041

**Nomenclature**

| | |
|---|---|
| $h_{sl}$ | latent heat of fusion [J kg$^{-1}$] |
| $k$ | thermal conductivity [W m$^{-1}$ °C$^{-1}$] |
| $q''$ | heat flux [W m$^{-2}$] |
| $q''_0$ | maximum heat flux [W m$^{-2}$] |
| $s$ | solid–liquid interface location [m] |
| $t$ | time [s] |
| $t_s$ | time at which solidification ends [s] |
| $t_p$ | half width of the laser beam pulse at $q''_0/2$ [s] |
| $T$ | temperature [°C] |
| $x$ | coordinate [m] |

*Greek symbols*

| | |
|---|---|
| $\alpha$ | thermal diffusivity [m$^2$ s$^{-1}$] |
| $\delta$ | thickness of thermal layer [m] |
| $\delta_s$ | thickness of thermal layer at the time at which solidification ends [m] |
| $\theta$ | temperature rise ($T - T_i$) [°C] |
| $\rho$ | density [kg m$^{-3}$] |
| $\tau$ | relative time, $t/t_p$ |
| $\tau_s$ | relative time at which solidification ends, $t_s/t_p$ |

*Subscripts*

| | |
|---|---|
| i | initial |
| l | liquid phase |
| m | melting point (when melting begins) |

melt pool size in a semi-infinite body due to a moving laser heat source. Kim and Sim [12] have studied thermal behavior and fluid flow during laser surface heating of alloys. Iwamoto et al. [13] have performed numerical analysis of energy transfer and surface modification of a metal surface by pulsed laser heating. While the above studies focused on long-pulse laser-material interactions, phase change heat transfer during ultrashort laser processing of metal films has also been investigated [14,15].

Laser-induced melting of metal powder in SLS processes differs from conventional melting because the loose powder can consist of as much as 40–60% gas. During melting it is necessary for the liquid phase to collect and drive the interstitial gasses out of the powder bed, effectively "shrinking" the volume of the powder bed. It is because of this shrinkage phenomenon that the powder bed experiences a significant density change during the melting process, resulting in motion of the surface of the powder bed during the SLS process. Melting of infinite and finite two-component metal powder beds subjected to constant heat flux was investigated by Zhang and Faghri [16] and Chen and Zhang [17]. An analytical solution of melting and resolidification of a two-component metal powder subjected to temporal Gaussian heat flux was obtained by Konrad et al. [18].

Although early research in SLS processes was conducted exclusively with Continuous Wave (CW) lasers, pulsed lasers with pulse widths ranging from milliseconds [19,20] to nanoseconds [21–23] have also recently been used to sinter metal powders. One advantage of pulsed laser sintering is that it can minimize the balling effect by decreasing the life span of the melt pool. Abe et al. [19] studied SLS of titanium powders using a YAG laser with pulse widths ranging from 1 to 5 ms and an average power of 50 W. Su et al. [20] investigated fully dense laser sintering of tool steel powder using a Nd:YAG laser with pulse widths between 0.5 and 20 ms and average power up to 550 W. The average power levels of the millisecond lasers used in Ref. [19,20] are comparable to that of a CW laser because the conduction heat loss into the unsintered region for a millisecond laser is similar to that of a CW laser.

The results of SLS experiments performed by Morgan et al. [21] on gas atomized 316L stainless steel using a nanosecond Nd:YAG laser showed that the vaporization recoil force overcame the surface tension forces acting on the melt, therefore improving the cohesion of the powder particles when compared to the CW SLS process. Fischer et al. [22,23] performed SLS experiments on titanium powder with a nanosecond Nd:YAG laser operated at a pulse width of 150 ns and repetition rate between 1 and 30 kHz. The powder grains could be joined at a much lower average temperature using moderate laser power, typically less than 10 W, as well as minimizing balling effects and introducing less residual stress in the workpiece [23]. When a pulsed Nd:YAG laser is used this process will yield higher lateral precision than the $CO_2$ process due to its shorter wavelength. In addition, the degree of partial melting and ultimately the local porosity in the final product can be easily controlled by several parameters, such as laser pulse, intensity, and repetition rate.

When a nanosecond laser is used to sinter metal powder, Fischer et al. [22–24] suggest that only a thin surface layer of the powder particle is melted and the core of the particle remains at its initial temperature. The temperature in the powder particle was estimated by a one-dimensional conduction model of a single spherical particle surrounded by a continuum that represents neighboring particles [24]. The time between pulses is long enough that thermalization can occur in the powder particle, leading to an average temperature that is higher than the previous initial temperature.

The model proposed by Fischer et al. [24] does not take into consideration the phase change of the powder grain and, since melting and resolidification are the mechanisms of this laser-based metal part manufacturing technique, their inclusion in any SLS model for metal powder is

essential. In order to discover the advantages of utilizing a pulsed laser in a SLS process, melting and resolidification of a single powder particle will be investigated in this paper. The effects of a change in laser pulse width, initial particle temperature, particle radius, and laser fluence on the simulation will also be investigated.

## 2. Physical model

Melting and resolidification of a single powder particle subjected to temporal Gaussian heat flux from a laser beam will be modeled. The diameter of the metal powder particle is much smaller than the diameter of the laser beam, which is in turn much smaller than the dimension of the final part. Since the laser radiation penetrates the powder bed over a distance of several powder-sphere diameters, it can be assumed that multiple scattering of the radiation leads to a nearly homogeneous distribution of the heat flux within the optically penetrated layer [24], which leads to an almost normal incidence of the radiation on the surfaces of the grains in the underlying layers. Fig. 1 shows the physical model of melting and resolidification under consideration. Due to symmetry of the spherical particle, the model can be assumed to be 1-D in the $r$-direction. The initial temperature of the powder particle, $T_i$, is well below its melting point. The origin of time is chosen as the time at which the heat flux is at its maximum, thus the time-dependent heat flux is

$$q''(t) = q''_0 \mathrm{e}^{-\ln 2 \frac{t^2}{t_p^2}} \tag{1}$$

where $t_p$ is the half-width of the laser pulse at half maximum.

The laser-powder grain interaction can be divided into three stages: (1) preheating, (2) melting and resolidification, and (3) thermalization. During the preheating period the powder grain must absorb sensible heat to raise its surface temperature to the melting point, $T_m$. During the melting and resolidification stage, the particle begins to melt and a thin skin of liquid, usually a few microns, forms on the surface of the powder sphere. In an actual SLS process, consolidation of the powder bed would occur during this stage because the liquid phase cannot maintain the relatively high initial porosity of the solid powder bed and therefore the interstitial gasses are driven from the powder bed. The surface heat flux reaches its maximum at the time $t = 0$, after which the heat flux will begin to decrease. The liquid layer will then be cooled by the particle's solid interior core, which acts as a heat sink, and eventually the partially melted particle resolidifies into a completely solid particle. At the time that the liquid pool has finished resolidification, the thermalization stage begins and the powder particle begins to thermalize to a uniform internal temperature. This uniform temperature is reached well before the next laser pulse occurs, and therefore the whole process can be modeled as a recurrence of the three stages by using the thermalized temperature of the powder particle from the previous pulse as the initial temperature in the preheating stage of the next pulse.

### 2.1. Governing equations

#### 2.1.1. Preheating stage

During preheating the heat transfer in the powder bed can be described as a pure conduction problem. The heat conduction equation in the powder bed is

$$\frac{\partial \theta_s}{\partial t} = \frac{\alpha_s}{(r_0 - x)^2} \frac{\partial}{\partial x}\left((r_0 - x)^2 \frac{\partial \theta_s}{\partial x}\right), \quad 0 \leqslant x \leqslant r_0, \ -\infty < t < t_m \tag{2}$$

subject to the following initial and boundary conditions:

$$\theta_s = 0, \quad 0 \leqslant x \leqslant r_0, \ t \to -\infty \tag{3}$$

$$\frac{\partial \theta_s}{\partial x} = 0, \quad x = r_0, \ -\infty < t < t_m \tag{4}$$

$$-k_s \frac{\partial \theta_s}{\partial x} = q''(t), \quad x = 0, \ -\infty < t < t_m \tag{5}$$

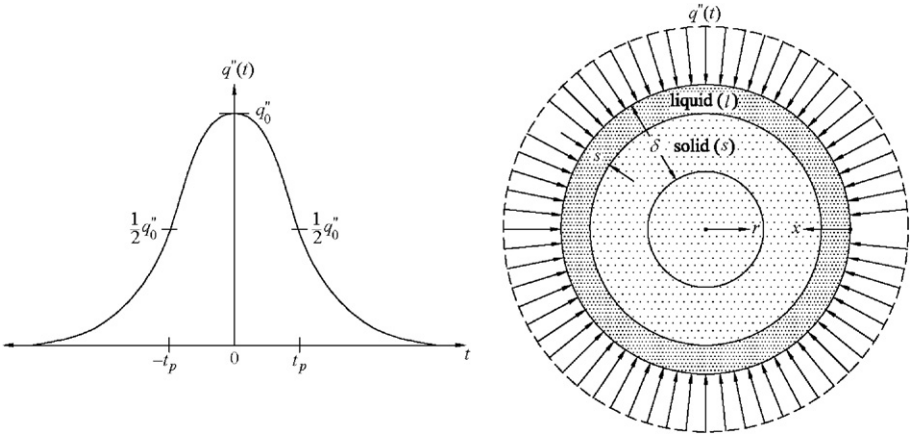


Fig. 1. The physical model.

*2.1.2. Melting and resolidification stage*

After melting has begun, $t \geqslant t_m$, the governing equation in the liquid phase is

$$\frac{\alpha_l}{(r_0-x)^2}\frac{\partial}{\partial x}\left((r_0-x)^2\frac{\partial\theta_l}{\partial x}\right)=\frac{\partial\theta_l}{\partial t},\quad 0<x<s(t),\ \ t_m<t<t_s \tag{6}$$

where $t_s$ is the time at which resolidification is complete and thermalization begins.

$$-k_l\frac{\partial\theta_l}{\partial x}=q''(t),\quad x=0,\ \ t_m<t<t_s \tag{7}$$

The energy equation in the solid phase is

$$\frac{\alpha_s}{(r_0-x)^2}\frac{\partial}{\partial x}\left((r_0-x)^2\frac{\partial\theta_s}{\partial x}\right)=\frac{\partial\theta_s}{\partial t},\quad s(t)<x<r_0,\ \ t_m<t<t_s \tag{8}$$

which is subjected to the following boundary conditions:

$$-k_l\frac{\partial\theta_l}{\partial x}+k_s\frac{\partial\theta_s}{\partial x}=\rho_s h_{sl}\frac{ds}{dt},\quad x=s(t),\ \ t_m<t<t_s \tag{9}$$

$$\theta_s(x,t)=\theta_l(x,t)=T_m-T_i,\quad x=s(t),\ \ t_m<t<t_s \tag{10}$$

$$\frac{\partial\theta}{\partial x}(x,t)=0,\quad x=r_0,\ \ t_m<t<t_s \tag{11}$$

*2.1.3. Thermalization stage*

After the liquid skin on the surface of the powder grain resolidifies there is still a temperature gradient within the particle. This stage can be described as a pure conduction problem with a non-uniform initial temperature distribution. The heat conduction equation in the powder bed is

$$\frac{\partial\theta}{\partial t}=\frac{\alpha_s}{(r_0-x)^2}\frac{\partial}{\partial x}\left((r_0-x)^2\frac{\partial\theta}{\partial x}\right),\quad 0\leqslant x\leqslant r_0,\ \ t>t_s \tag{12}$$

Since the resolidification stage is not complete until several pulse widths after the peak heat flux at the surface occurs, the laser beam's Gaussian distribution allows for the assumption that heat flux at the surface is negligible at this late time in the simulation. The boundary conditions of the thermalization stage are therefore

$$\frac{\partial\theta}{\partial x}=0,\quad x=0,\ \ t>t_s \tag{13}$$

$$\frac{\partial\theta}{\partial x}=0,\quad x=r_0,\ \ t>t_s \tag{14}$$

The temperature profile within the particle must also be continuous at the time $t=t_s$, therefore

$$\theta(x,t=t_s^-)=\theta(x,t=t_s^+) \tag{15}$$

a condition which will be discussed further in the solution section.

## 3. The integral approximate solution

When the surface of the powder particle is exposed to heat flux the heat will penetrate the surface and begin to conduct inward. The depth to which the heat flux has penetrated is referred to as the thermal penetration depth, $\delta$, beyond which the temperature is equal to the initial temperature. Therefore, the following two boundary conditions are valid for all stages:

$$\theta_s(x,t)=0,\quad x\geqslant\delta(t),\ \ t>-\infty \tag{16}$$

$$\frac{\partial\theta_s}{\partial x}=0,\quad x\geqslant\delta(t),\quad t>-\infty \tag{17}$$

*3.1. Solution for the preheating stage*

As the heat flux penetrates the surface of the particle the thermal penetration depth, $\delta$, will increase. Since the powder particle has a finite radius, it is probable that at some point during the preheating stage the thermal penetration depth will reach the center of the particle. If this is the case then there will be two separate solutions for the preheating stage, one solution for $\delta<r_0$ and one for $\delta=r_0$, both of which are included below. It will also be necessary to monitor the temperature at the surface of the powder particle, $\theta_s(0,t)$, so that the onset of melting can be detected.

*3.1.1. Solution for the preheating stage with $\delta < r_0$*

Integrating both sides of Eq. (2) with respect to $x$ in the interval of $(0,\delta)$ and applying Eqs. (5), (16) and (17), the integral energy equation becomes

$$\frac{\partial}{\partial t}\int_0^\delta(r_0-x)^2\theta_s(x,t)\,dx=\frac{\alpha_s q_0'' r_0^2}{k_s}e^{-\ln 2\frac{t^2}{t_p^2}} \tag{18}$$

Assuming that the temperature distribution can be approximated by a second degree polynomial function and solving the unknown constants using the boundary conditions of Eqs. (5), (16) and (17), the temperature distribution in the thermal penetration depth becomes

$$\theta_s(x,t)=\frac{q_0''(\delta-x)^2}{2k_s\delta}e^{-\ln 2\frac{t^2}{t_p^2}},\quad \delta<r_0,\ \ t<t_m \tag{19}$$

Substituting Eq. (19) into Eq. (18) yields

$$\frac{\partial}{\partial t}\left[\frac{1}{6}\delta^2 e^{-\ln 2\frac{t^2}{t_p^2}}\left(r_0^2-\frac{1}{2}r_0\delta+\frac{1}{10}\delta^2\right)\right]=\alpha_s r_0^2 e^{-\ln 2\frac{t^2}{t_p^2}} \tag{20}$$

which is subject to the initial condition of $\delta=0$, $t=-\infty$.

Integrating Eq. (20) with respect to $t$ in the interval $(-\infty,t)$ one obtains

$$0=\frac{1}{60}\delta^4 e^{-\ln 2\frac{t^2}{t_p^2}}-\frac{1}{12}\delta^3 r_0 e^{-\ln 2\frac{t^2}{t_p^2}}+\frac{1}{6}\delta^2 r_0^2 e^{-\ln 2\frac{t^2}{t_p^2}}-\frac{\alpha_s r_0^2 t_p\sqrt{\pi}}{2\sqrt{\ln 2}}\left[1+\operatorname{erf}\left(\sqrt{\ln 2}\frac{t}{t_p}\right)\right],\quad \delta<r_0,\ \ t<t_m \tag{21}$$

Only one of the four roots of Eq. (21) will be both real and positive and this root will be the value of $\delta$ for the particular time.

*3.1.2. Solution for the preheating stage with $\delta = r_0$*

When $\delta$ reaches the center of the powder particle the boundary conditions of Eqs. (16) and (17) will no longer be useful. Assuming that the temperature distribution can be approximated by a second degree polynomial and determining the constants using Eqs. (4) and (5), the temperature distribution in the particle becomes [25]

$$\theta_s(x,t) = \frac{q''_0(r_0-x)^2}{2k_s r_0} e^{-\ln 2\frac{t^2}{t_p^2}} + T_c(t) - T_i, \quad \delta = r_0, \ \ t < t_m \tag{22}$$

The integral energy equation in this stage can be obtained by integrating both sides of Eq. (2) with respect to $x$ in the interval of $(0, r_0)$ and applying Eqs. (4) and (5), i.e.,

$$\frac{\partial}{\partial t}\int_0^{r_0}(r_0-x)^2\theta_s(x,t)\,dx = \frac{\alpha_s q'' r_0^2}{k_s} e^{-\ln 2\frac{t^2}{t_p^2}} \tag{23}$$

Substituting Eq. (22) into Eq. (23) yields

$$\frac{\partial}{\partial t}\left[\frac{q''_0 r_0^4}{10k_s} e^{-\ln 2\frac{t^2}{t_p^2}} + \frac{1}{3}r_0^3(T_c(t)-T_i)\right] = \frac{\alpha_s q''_0 r_0^2}{k_s} e^{-\ln 2\frac{t^2}{t_p^2}} \tag{24}$$

which is subject to the initial condition of $T_c(t) = T_i$, $t = t_\delta$, where $t_\delta$ is the time at which $\delta$ reaches$r_0$, the center of the particle. Eq. (24) can be integrated with respect to $t$ in the interval $(t_\delta, t)$ to yield

$$\frac{q''_0 r_0^4}{10k_s}\left[e^{-\ln 2\frac{t^2}{t_p^2}} - e^{-\ln 2\frac{t_\delta^2}{t_p^2}}\right] + \frac{1}{3}r_0^3(T_c(t)-T_i) = \frac{q''_0\alpha_s r_0^2 t_p\sqrt{\pi}}{2k_s\sqrt{\ln 2}}\left[\operatorname{erf}\left(\sqrt{\ln 2}\frac{t}{t_p}\right) - \operatorname{erf}\left(\sqrt{\ln 2}\frac{t_\delta}{t_p}\right)\right], \quad \delta = r_0, \ \ t < t_m \tag{25}$$

Solving for $T_c(t) - T_i$ from Eq. (25) and substituting the result into Eq. (22), the temperature distribution becomes

$$\theta_s(x,t) = \frac{q''_0(r_0-x)^2}{2k_s r_0} e^{-\ln 2\frac{t^2}{t_p^2}} - \frac{3q''_0 r_0}{10k_s}\left[e^{-\ln 2\frac{t^2}{t_p^2}} - e^{-\ln 2\frac{t_\delta^2}{t_p^2}}\right] + \frac{3q''_0\alpha_s t_p\sqrt{\pi}}{2k_s r_0\sqrt{\ln 2}}\left[\operatorname{erf}\left(\sqrt{\ln 2}\frac{t}{t_p}\right) - \operatorname{erf}\left(\sqrt{\ln 2}\frac{t_\delta}{t_p}\right)\right], \quad \delta = r_0, \ \ t < t_m \tag{26}$$

### 3.2. Solution for the melting and solidification stage

*3.2.1. Solution for the solid region*

After the temperature at the surface of the powder particle reaches the melting point the preheating stage ends and the melting and resolidification stage begins. Even though melting has begun, the solution for the solid region is sill needed in the heat affected zone between the solid–liquid interface, $s$, and the thermal penetration depth, $\delta$. The following procedure is nearly identical to that of the preheating stage solution, the principal change being the limits of integration.

Integrating both sides of Eq. (8) with respect to $x$ in the interval of $(s, \delta)$ and applying Eqs. (10), (16), and (17), the integral energy equation becomes

$$\frac{\partial}{\partial t}\int_s^\delta (r_0-x)^2\theta_s(x,t)\,dx + (T_m - T_i)(r_0-s)^2\frac{\partial s}{\partial t} = -\alpha_s(r_0-s)^2\frac{\partial\theta_s}{\partial x}\bigg|_s \tag{27}$$

Assuming a second-degree polynomial temperature distribution and solving the unknown constants using the boundary conditions of Eqs. (10), (16), and (17), the temperature distribution in the thermal penetration depth becomes

$$\theta_s(x,t) = \frac{(T_m - T_i)}{(\delta - s)^2}(\delta - x)^2, \quad \delta < r_0, \ \ t_m < t < t_s \tag{28}$$

Substituting Eq. (28) into Eq. (27) yields

$$0 = 30(r_0-s)^2\frac{\partial s}{\partial t} - 60\alpha_s\frac{(r_0-s)^2}{(\delta-s)} + \frac{\partial}{\partial t}\left[-10r_0^2 s + 15r_0 s^2 - 6s^3 + 10r_0^2\delta - 10r_0 s\delta + 3s^2\delta - 5r_0\delta^2 + 2s\delta^2 + \delta^3\right] \tag{29}$$

which is subject to the initial conditions of $\delta(t) = \delta_m$ and $s(t) = 0$ at $t = t_m$.

Integrating Eq. (29) with respect to $t$ in the interval $(t_m, t)$ and collecting terms for $\delta$ one obtains

$$0 = \delta^3[1] + \delta^2[-5r_0 + 2s] + \delta^1[10r_0^2 - 10r_0 s + 3s^2] + \delta^0\left[-15r_0 s^2 + 20r_0^2 s + 4s^3 - 10r_0^2\delta_m + 5r_0\delta_m^2 - \delta^3 - 60\alpha_s\int_{t_m}^t\frac{(r_0-s)^2}{(\delta-s)}\,dt\right], \quad \delta < r_0, \ \ t_m < t < t_s \tag{30}$$

Only one of the roots of Eq. (30) will be both real and positive and this root will be the value of $\delta$ for the particular time.

*3.2.2. Solution for the liquid region*

By assuming a temperature distribution of the form $\theta_l(x,t) = A_l/(r_0 - x) + B_l$ and using the boundary conditions of Eqs. (7) and (10) to determining $A_l$ and $B_l$, one obtains

$$\theta_l(x,t) = \frac{q''_0 r_0^2}{k_l} e^{-\ln 2\frac{t^2}{t_p^2}}\left[\frac{1}{r_0 - s} - \frac{1}{r_0 - x}\right] + (T_m - T_i), \quad t_m < t < t_s, \ \ 0 < x < \delta \tag{31}$$

Substituting Eqs. (28) and (31) into Eq. (9) and integrating the resulting equation with respect to $t$ in the interval of $t_m$ to $t$, one obtains

$$s = \frac{q''_0 r_0^2}{h_{sl}\rho_s}\int_{t_m}^t\frac{1}{(r_0-s)^2}e^{-\ln 2\frac{t^2}{t_p^2}}\,dt - \frac{2k_s(T_m - T_i)}{h_{sl}\rho_s}\int_{t_m}^t\frac{1}{(\delta - s)}\,dt \tag{32}$$

which must be evaluated numerically during the simulation because of the presence of $s$ on the right-hand side.

### 3.3. Solution for the thermalization stage

At the time that thermalization stage begins, the temperature distribution within the particle is

$$\theta(x,t_s)=\begin{cases}\frac{T_m-T_i}{\delta_s^2}(\delta_s-x)^2, & 0<x<\delta_s\\ 0, & \delta_s<x<r_0\end{cases} \tag{33}$$

which is the initial condition for the thermalization stage. The heat transfer in the thermalization stage is governed by Eqs. 12,13,14 and (33). In order to satisfy Eq. (33), the thermalization problem can be decomposed into the two sub-problems:

$$\theta=\theta_1+\theta_2 \tag{34}$$

where both $\theta_1$ and $\theta_2$ satisfy Eq. (12). The boundary and initial conditions of $\theta_1$ are

$$\frac{\partial\theta_1}{\partial x}=\frac{-2(T_m-T_i)}{\delta_s},\quad x=0,\ t_s<t<t_{therm} \tag{35}$$

$$\frac{\partial\theta_1}{\partial x}=0,\quad x=r_0,\ t_s<t<t_{therm} \tag{36}$$

$$\theta_1(x,t=t_s)=\begin{cases}\frac{T_m-T_i}{\delta_s^2}(\delta_s-x)^2, & 0<x<\delta_s\\ 0, & \delta_s<x<r_0\end{cases} \tag{37}$$

and the boundary and initial conditions of $\theta_2$ are

$$\frac{\partial\theta_2}{\partial x}=-\frac{\partial\theta_1}{\partial x}=\frac{2(T_m-T_i)}{\delta_s},\quad x=0,\ t_s<t<t_{therm} \tag{38}$$

$$\frac{\partial\theta_2}{\partial x}=0,\quad x=r_0,\ t_s<t<t_{therm} \tag{39}$$

$$\theta_2(x,t)=0,\quad 0<x<r_0,\ t=t_s \tag{40}$$

#### 3.3.1. Solution of sub-problem for $\theta_1$

The solution of the $\theta_1$ sub-problem is independent of the $\theta_2$ sub-problem and can be obtained using the integral approximate method. By following a procedure similar to that of the preheating stage, the solution of the $\theta_1$ sub-problem for $\delta_1<r_0$ is

$$\theta_1(x,t)=\frac{(T_m-T_i)}{\delta_s\delta_1}(x-\delta_1)^2,\quad \delta_1<r_0 \tag{41}$$

where $\delta_1$ can be obtained from

$$0=\delta_1^4-5r_0\delta_1^3+10r_0^2\delta_1^2-\delta_s^4+5r_0\delta_s^3-10r_0^2\delta_s^2-60\alpha_s r_0^2(t-t_s),\quad \delta_1<r_0 \tag{42}$$

Only one root of this polynomial will be both real and positive, and this will be the value of $\delta_1$ at each time step until $\delta_1$ reaches the center of the particle, $r_0$.

After the thermal penetration depth, $\delta_1$, reaches the center of the particle, $\theta_1$ can be obtained using an integral solution

$$\theta_1(x,t)=\frac{6\alpha_s(T_m-T_i)}{r_0\delta_s}(t-t_{1r_0})+\frac{(T_m-T_i)}{r_0\delta_s}(r_0-x)^2,\quad \delta_1=r_0 \tag{43}$$

where $t_{1r_0}$ is the time at which $\delta_1$ reaches the center of the powder particle.

#### 3.3.2. Solution of the sub-problem for $\theta_2$

Since the initial temperature of the second sub-problem is uniform [see Eq. (40)] its thermal penetration depth, $\delta_2$, will originate from the surface at the time $t=t_s$ and begin to penetrate the particle. Before $\delta_2$ reaches the center of the particle, $\theta_2$ can be obtained using the integral approximate solution, the result of which is

$$\theta_2=-\frac{(T_m-T_i)}{\delta_2\delta_s}(x-\delta_2)^2,\quad \delta_2<r_0 \tag{44}$$

A value for $\delta_2$ at each time step in the simulation can be obtained from the roots of the polynomial

$$0=\delta_2^4-5r_0\delta_2^3+10r_0^2\delta_2^2-60\alpha_s r_0^2(t-t_s),\quad \delta_2<r_0 \tag{45}$$

After $\delta_2$ has reached the center of the particle, $\theta_2$ can be obtained from the integral approximate solution as

$$\theta_2(x,t)=\frac{-6\alpha_s(T_m-T_i)}{r_0\delta_s}(t-t_{2r_0})-\frac{(T_m-T_i)}{r_0\delta_s}(r_0-x)^2,\quad \delta_2=r_0 \tag{46}$$

where $t_{2r_0}$ is the time at which $\delta_2$ reaches the center of the powder particle.

## 4. Results and discussion

After solving the heat transfer problem in terms of various system parameters it is necessary to adapt this solution to use the parameters that describe common laser apparatuses. The heat flux at the particle surface, $q''$ (W/m$^2$) can be related to the total energy input to the powder particle by one pulse, or the laser fluence $J$ (J/m$^2$):

$$J=\int_{-\infty}^{\infty}q''(t)\,dt=\int_{-\infty}^{\infty}q_0''e^{-\ln 2\frac{t^2}{t_p^2}}dt=q_0''t_p\frac{2\sqrt{\pi}}{\sqrt{\ln 2}} \tag{47}$$

Now the simulation parameters can be varied via a computer simulation in order to determine the impact they would have on the phase change of a single titanium powder particle.

Fig. 2 shows the surface temperature of the powder particle for a time span of 400 μs. The laser pulse frequency of 5000 Hz corresponds to 200 μs between laser pulses, as we can see from the figure. The first pulse, which occurs at 100 μs, raises the surface temperature of the powder particle from the initial temperature of 293–1952 K, a temperature one degree below the melting temperature of the titanium powder particle. After the laser pulse the temperature gradient within the particle thermalizes to a uniform internal temperature of 830 K where it remains until the next laser pulse occurs at 300 μs. This laser pulse heats the surface of the powder particle to its melting point of 1953 K, at which time melting begins and a thin skin of liquid develops on the surface. The second laser pulse then

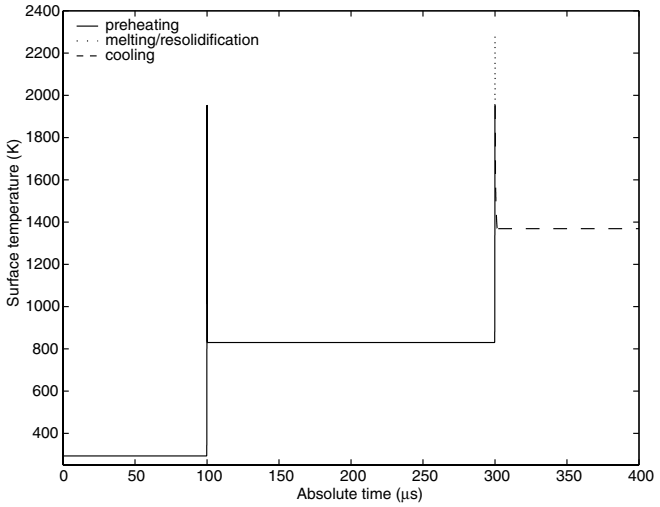


Fig. 2. Particle surface temperature versus time for two laser pulses ($J = 9320$ J/m$^2$, $t_p = 75$ ns, $r_0 = 11$ μm, $f = 5000$ Hz).

continues to heat the particle surface to a peak temperature of 2286 K after which the liquid skin cools, resolidifies, and eventually thermalizes to a uniform temperature of 1367 K.

Fig. 3 details what happens to the powder grain during the first laser pulse shown in Fig. 2. Fig. 3(a) shows the excess temperature, $\theta = T - T_i$, of the particle at both the surface and the center versus dimensionless time $\tau = t/t_p$. Fig. 3(b) shows the variations location of the thermal penetration depth, $\delta$, versus dimensionless time $\tau$. As the flux at the surface increases, excess surface temperature and thermal penetration depth also increase. After the peak heat flux occurs the surface temperature begins to fall as the particle thermalizes. When the thermal penetration depth reaches the center of the particle at the time $\tau = 1.75$ the temperature at the center of the particle begins to rise. The two curves converge at the time $\tau = 3.20$, at which time the particle has reached a uniform internal temperature 537 K higher than its initial temperature. Since the energy delivered to the particle with each laser pulse is a constant, the change in temperature will be the same for each pulse regardless of the previous initial grain temperature. Therefore, assuming that melting does not occur, the particle temperature after a number of pulses can easily be predicted by multiplying the temperature rise per pulse by the number of pulses to which the particle is subjected.

Fig. 4 shows the temperature profile within the powder particle at various times during the simulation for the baseline values. It shows an increase in temperature throughout the powder particle as the process continues. The line corresponding to $\tau = \tau_{peak}$ is the time at which the surface of the powder particle reaches its maximum temperature, the time $\tau = \tau_s$ represents the time at which the liquid skin on the surface of the particle finishes solidification, and the time $\tau = \tau_{therm}$ represents the time at which the particle has finished thermalization. Note the uniform internal temperature at this time. The progression of the thermal penetration depth during the duration of the process can also be seen in the figure.

Fig. 5 shows the effect of a change in laser pulse width, $t_p$, on the simulation process. By examining Eq. (47) one sees that a decrease in $t_p$ also results in an increase in heat flux, $q''_0$, if laser fluence $J$ is to be held constant. A shorter laser pulse width results in quicker delivery of the laser pulse's energy and, as the plot shows, an increase in surface temperature, a decrease in the time necessary for melting to begin, and an increase in the time necessary for resolidification. Since the same amount of energy input to the particle is unchanged the final thermalized temperature will be unaffected, as shown by Fig. 5. Fig. 6 shows the effect of a change in laser pulse width on the location of the solid–liquid interface. It can be seen from the figure that, analytically, when the laser pulse widths are limited to the range of 60–90 ns and evaporation at the surface of

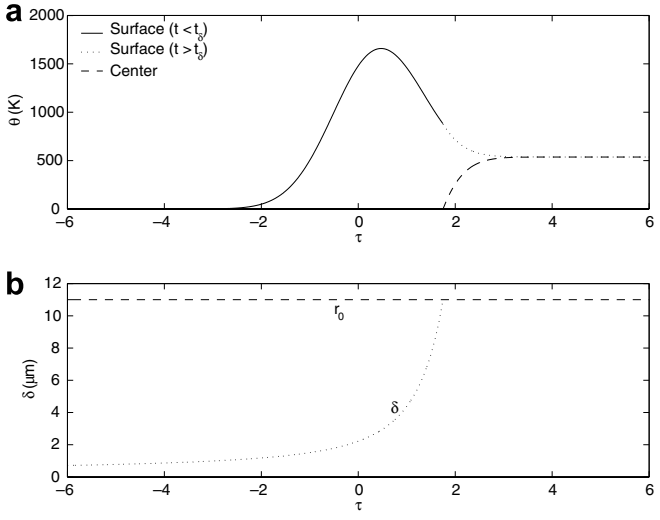


Fig. 3. Surface temperature and thermal penetration depth during the preheating phase ($J = 9320$ J/m$^2$, $t_p = 75$ ns, $r_0 = 11$ μm, $f = 5000$ Hz). (a) Temperatures. (b) Thermal penetration depth.

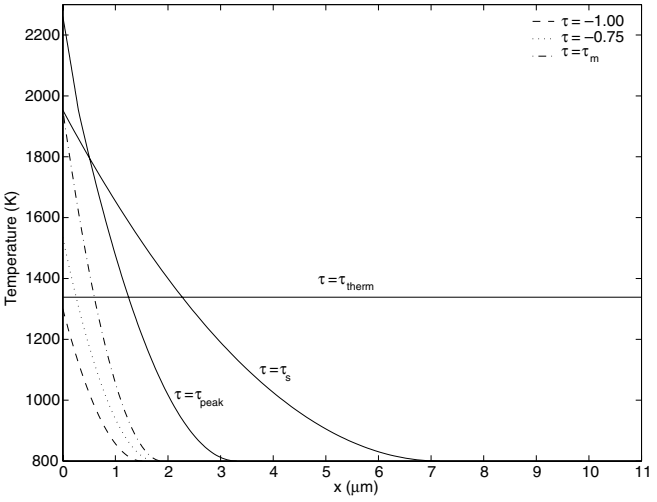


Fig. 4. The temperature profile within the powder particle at various times during the simulation ($J = 9320$ J/m$^2$, $t_p = 75$ ns, $r_0 = 11$ μm, $f = 5000$ Hz, $T_i = 800$ K).

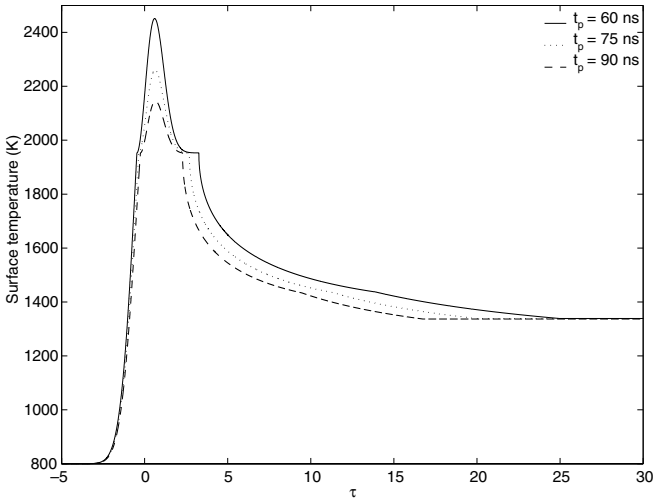


Fig. 5. Surface temperature versus time for various values of laser pulse width ($J = 9320$ J/m$^2$, $r_0 = 11$ μm, $f = 5000$ Hz, $T_i = 800$ K).

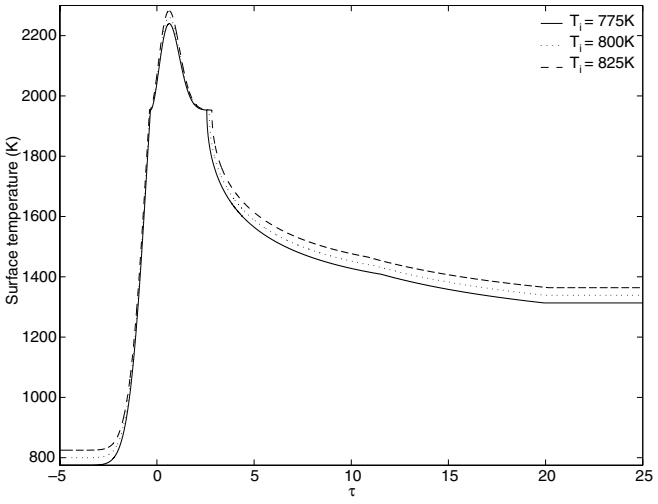


Fig. 7. Surface temperature versus time for various values of initial particle temperature ($J = 9320$ J/m$^2$, $t_p = 75$ ns, $r_0 = 11$ μm, $f = 5000$ Hz).

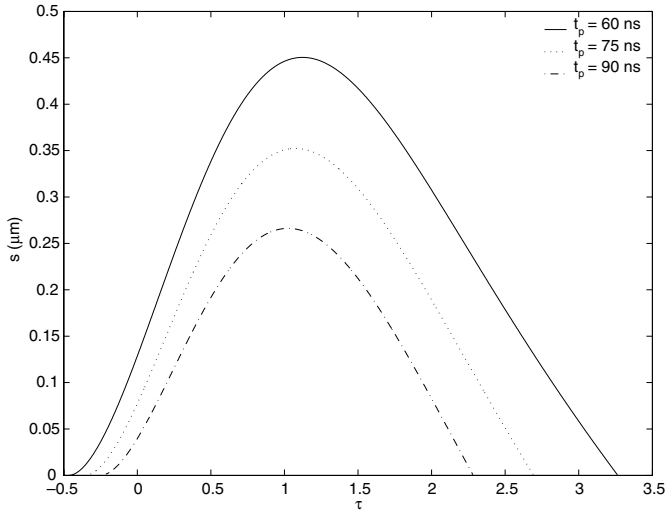


Fig. 6. The location of the solid–liquid interface versus time for various values of laser pulse width ($J = 9320$ J/m$^2$, $r_0 = 11$ μm, $f = 5000$ Hz, $T_i = 800$ K).

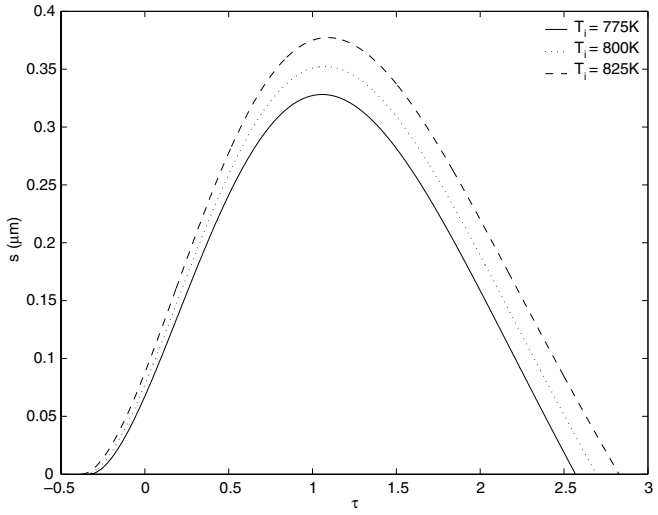


Fig. 8. The location of the solid–liquid interface versus time for various values of initial particle temperature ($J = 9320$ J/m$^2$, $t_p = 75$ ns, $r_0 = 11$ μm, $f = 5000$ Hz).

the particle is not present, a shorter pulse width results in more melted material and as a result increases both the time necessary for the particle to resolidify and the time necessary for the particle to thermalize. In "real life," however, it has been observed that shorter pulses at the same fluence eventually raise the temperature of the surface layer to its evaporation point before melt can be produced.

The effect of the particle initial temperature on the simulation is seen in Figs. 7 and 8. If the initial temperature of the powder particle is increased then the laser must do less preheating and thus melting will occur sooner, a higher surface temperature will be reached, and more material will be melted. More melted material will take longer to resolidify and thus thermalization time will be increased. For obvious reasons the final thermalized particle temperature also increases as initial temperature increases.

Fig. 9 shows that a smaller powder particle will reach a higher surface temperature than a larger one. This makes sense when one considers that even though the amount of energy deposited on all three spheres is the same, the smaller sphere has less mass to heat and thus reaches a higher temperature than the larger one. This is also the reason that the final temperature of the smaller sphere is higher than that of a larger sphere. In addition, a smaller sphere will thermalize faster than a larger sphere because the heat has less material to penetrate. Fig. 10 shows that the size of the powder particle does not have a significant effect on the time necessary for melting to begin, however, a smaller powder particle experiences more melting than a larger one and thus takes longer to solidify. Although a discrepancy exists where peak temperatures are concerned, the thermalized temperatures of the spheres are all the same.

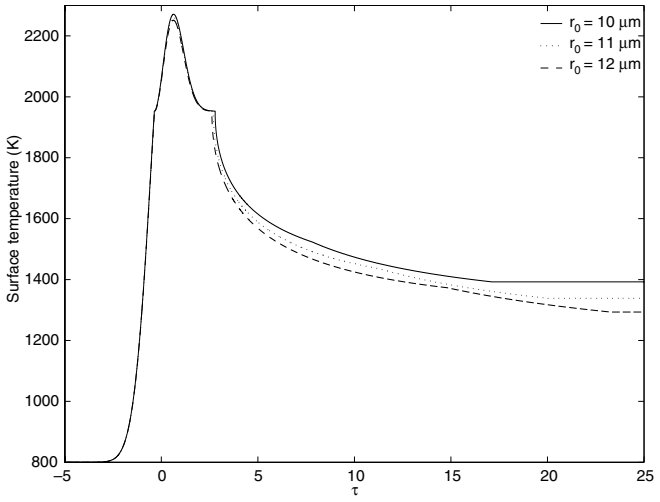


Fig. 9. Surface temperature versus time for various values of particle radius ($J = 9320$ J/m$^2$, $t_p = 75$ ns, $f = 5000$ Hz, $T_i = 800$ K).

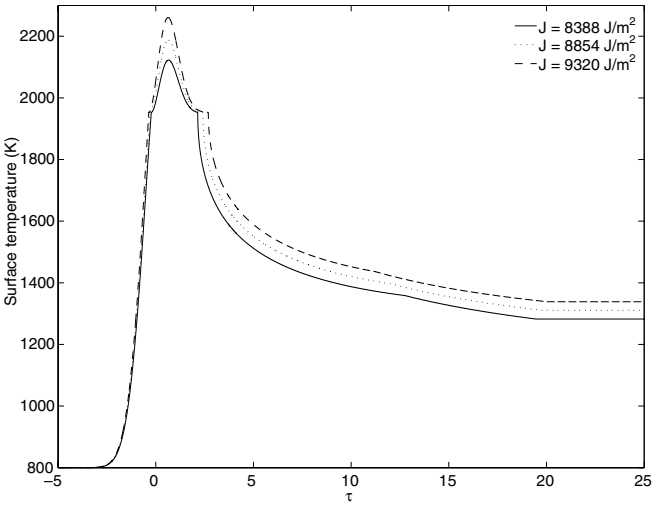


Fig. 11. Surface temperature versus time for various values of laser fluence ($t_p = 75$ ns, $r_0 = 11$ μm, $f = 5000$ Hz, $T_i = 800$ K).

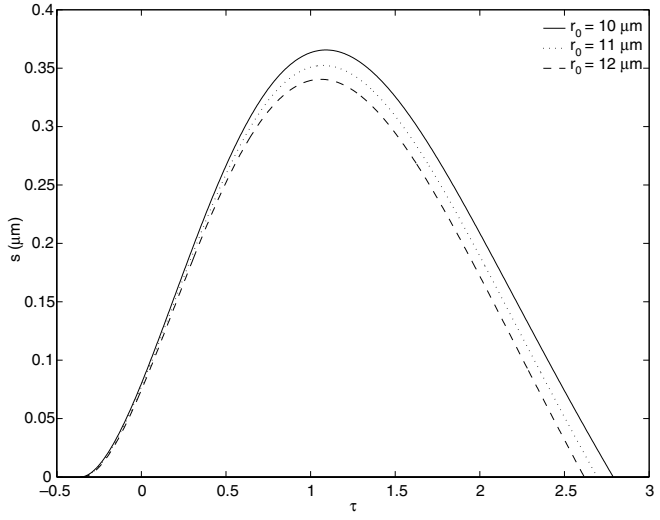


Fig. 10. The location of the solid liquid interface versus time for various values of particle radius ($J = 9320$ J/m$^2$, $t_p = 75$ ns, $f = 5000$ Hz, $T_i = 800$ K).

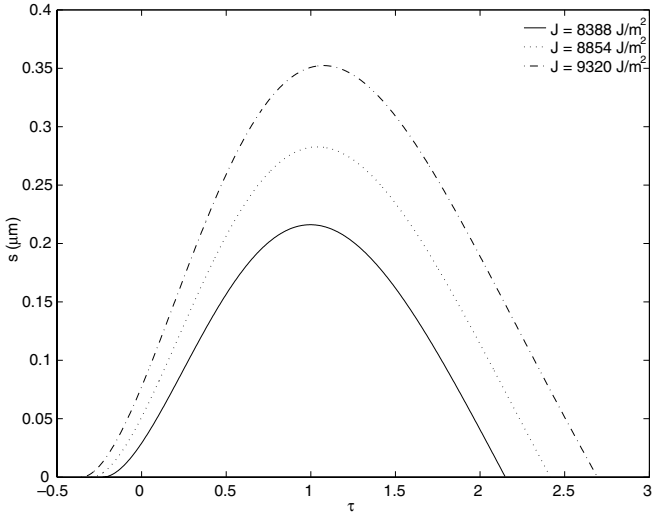


Fig. 12. The location of the solid–liquid interface versus time for various values of laser fluence ($t_p = 75$ ns, $r_0 = 11$ μm, $f = 5000$ Hz, $T_i = 800$ K).

Fig. 11 shows the effect of a change in laser fluence, $J$, on the temperature experienced at the surface of the powder grain. The 5% increase in laser fluence, which is essentially a 5% increase in $q''_0$ according to Eq. (47), shown in the figure results in a dramatic increase in surface temperature and increases the time it takes for the liquid skin of the particle to resolidify. With an increase in laser fluence the time necessary for melting to begin decreases and the time necessary for the particle to thermalize increases. The effect of a change in laser fluence on the location of the solid–liquid interface can be observed in Fig. 12. Clearly an increase in laser fluence results in a larger amount of melted material causing the previously mentioned increase in time necessary for solidification to occur. Finally, an increase in laser fluence, the total amount of energy deposited on the sphere during the pulse, will obviously result in an increase in the final thermalized temperature of the sphere.

## 5. Conclusion

Melting and resolidification in a subcooled powder particle with temporal Gaussian heat flux was investigated analytically. It is clear that laser fluence is the most important processing parameter; however, other parametric changes also have effects on the results of the phase change process. The effect of a decrease in either particle radius or laser pulse width or an increase in either laser fluence or initial particle temperature is the same, namely an earlier melting time, a higher surface temperature, more melted material, and a longer solidification time. The physical

model and results of this investigation pave the way for further modeling of SLS processes with a pulsed laser.

## Acknowledgements

Support for this work by the Office of Naval Research (ONR) under grant number N00014-04-1-0303 and by the University of Missouri Research Board is gratefully acknowledged.

## References

[1] M. Agarwala, D. Bourell, J. Beaman, H. Marcus, J. Barlow, Direct selective laser sintering of metals, Rapid Prototyping J. 1 (1) (1995) 26–36.
[2] S. Das, J. Beaman, M. Wohlert, D. Bourell, Direct laser freeform fabrication of high performance metal components, Rapid Prototyping J. 4 (3) (1998) 112–117.
[3] S. Kumar, Selective laser sintering: a qualitative and objective approach, JOM 55 (10) (2003) 43–47.
[4] N.K. Tolochko, S.E. Mozzharov, I.A. Yadroitsev, T. Laoui, L. Froyen, V.I. Titov, M.B. Ignatiev, Balling processes during selective laser treatment of powders, Rapid Prototyping J. 10 (2) (2004) 78–87.
[5] D.E. Bunnell, Fundamentals of selective laser sintering of metals, PhD thesis, University of Texas at Austin, Austin, TX, 1995.
[6] T. Manzur, T. DeMaria, W. Chen, C. Roychoudhuri, Potential role of high power laser diode in manufacturing, in: SPIE Photonics West Conference, San Jose, CA, 1996.
[7] R. Viskanta, Phase change heat transfer, in: G.A. Lane (Ed.), Solar Heat Storage: Latent Heat Materials, CRC Press, Boca Raton, FL, 1983.
[8] L.S. Yao, J. Prusa, Melting and freezing, Adv. Heat Transfer 19 (1989) 1–95.
[9] A. Faghri, Y. Zhang, Transport Phenomena in Multiphase Systems, Elsevier, Burlington, MA, 2006.
[10] B.S. Yilbas, Study into a numerical solution for a pulsed $CO_2$ laser heating process, Numer. Heat Transfer Part A 28 (4) (1995) 487–502.
[11] A.A. Rostaml, A. Raisi, Temperature distribution and melt pool size in a semi-infinite body due to a moving laser heat source, Numer. Heat Transfer, Part A 31 (7) (1997) 783–796.
[12] W.S. Kim, B.C. Sim, Study of thermal behavior and fluid flow during laser surface heating of alloys, Numer. Heat Transfer, Part A 31 (7) (1997) 703–723.
[13] M. Iwamoto, M. Ye, C.P. Grigoropoulos, R. Grief, Numerical analysis of pulsed laser heating for the deformation of metals, Numer. Heat Transfer Part A 34 (8) (1998) 791–804.
[14] J.K. Chen, J.E. Beraun, Numerical study of ultrashort laser pulse Interactions with metal films, Numer. Heat Transfer Part A 40 (1) (2001) 1–20.
[15] I.H. Chowdhury, X. Xu, Heat transfer In femtosecond laser processing of metal, Numer. Heat Transfer, Part A 44 (3) (2003) 219–232.
[16] Y. Zhang, A. Faghri, Melting of a subcooled mixed powder bed with constant heat flux heating, Int. J. Heat Mass Transfer 42 (5) (1999) 775–788.
[17] T. Chen, Y. Zhang, Analysis of melting in a subcooled two-component metal powder layer with constant heat flux, Appl. Therm. Eng. 26 (7) (2006) 751–765.
[18] C. Konrad, Y. Zhang, B. Xiao, Analysis of melting and resolidification in a two-component metal powder bed subjected to temporal Gaussian heat flux, Int. J. Heat Mass Transfer 48 (19-20) (2005) 3932–3944.
[19] F. Abe, E. Costa Santos, Y. Kitamura, K. Osakada, M. Shiomi, Influence of forming conditions on the titanium model in rapid prototyping with the selective laser melting process, Proc. Inst. Mech. Eng. Part C – J. Mech. Eng. Sci. 217 (1) (2003) 119–126.
[20] W-N Su, P. Erasenthiran, P.M. Dickens, Investigation of fully dense laser sintering of tool steel powder using a pulsed Nd: YAG (neodymium-doped yttrium aluminium garnet) laser, Proc. Inst. Mech. Eng. Part C – J. Mech. Eng. Sci. 217 (1) (2003) 127–138.
[21] R. Morgan, C.J. Sutcliffe, W. O'Neill, Experimental investigation of nanosecond pulsed Nd:YAG laser re-melted pre-placed powder beds, Rapid Prototyping J. 7 (3) (2001) 159–172.
[22] P. Fischer, V. Romano, H.P. Weber, N.P. Karapatis, E. Boillat, R. Glardon, Sintering of commercially pure titanium powder with a Nd:YAG laser source, Acta Mater. 51 (6) (2003) 1651–1662.
[23] P. Fischer, V. Romano, H.P. Weber, S. Kolossov, Pulsed laser sintering of metallic powders, Thin Solid Films 453–454 (2004) 139–144.
[24] P. Fischer, N. Karapatis, V. Romano, R. Glardon, H.P. Weber, A model for the interaction of near-infrared laser pulses with metal powders in selective laser sintering, Appl. Phys. A 74 (4) (2002) 467–474.
[25] L.A. Dombrovsky, S.S. Sazhin, A simplified non-isothermal model for droplet heating and evaporation, Int. Commun. Heat Mass Transfer 30 (6) (2003) 787–796.